Inorganic Chemistry

Article

pubs.acs.org/IC

# K–$H_3C$ and K–Sn Interactions in Potassium Trimethylstannyl Complexes: A Structural, Mechanochemical, and NMR Study

Christian Kleeberg,*[,†] Jörg Grunenberg,*[,‡] and Xiulan Xie*[,§]

[†]Institut für Anorganische und Analytische Chemie, Technische Universität Carolo-Wilhelmina zu Braunschweig, Hagenring 30, 38106 Braunschweig, Germany

[‡]Institut für Organische Chemie, Technische Universität Carolo-Wilhelmina zu Braunschweig, Hagenring 30, 38106 Braunschweig, Germany

[§]Fachbereich Chemie, Philipps-Universität Marburg, Hans-Meerwein-Straße, 35043 Marburg, Germany

Supporting Information

**ABSTRACT:** A series of trimethylstannyl potassium complexes $[K(L)SnMe_3]$ with different auxiliary ligands L (L = 18-C-6, $(TMEDA)_2$ (TMEDA = tetramethylethylenediamine), and $(12\text{-}C\text{-}4)_2$) were synthesized by alkoxide-induced B–Sn bond cleavage. X-ray structure determinations were performed for all these complexes, and the structural chemistry was studied in detail. For L = 18-C-6 and $(TMEDA)_2$ the solid state structures comprise polymeric $[K(L)SnMe_3]_n$ chains containing bidentate trimethylstannyl anions bridging two $[K(L)]^+$ ions, featuring unsymmetrical coordination of the $[K(L)]^+$ ion by K–Sn and K–$H_3C$ interactions as a central structural motif. In contrast, for L = $(12\text{-}C\text{-}4)_2$, separated $[K(12\text{-}C\text{-}4)_2]^+$ and $[SnMe_3]^-$ ions are observed. Unexpectedly, in the presence of tetrahydrofuran (THF), $[K(18\text{-}C\text{-}6)SnMe_3]_n$ forms upon crystallization a new species consisting of separated $[K(18\text{-}C\text{-}6)(THF)_2]^+$ and $[(Me_2SnCH_3)K(18\text{-}C\text{-}6)SnMe_3]^-$ ions. In this unsymmetrical anion two trimethylstannyl anions coordinate a single $[K(18\text{-}C\text{-}6)]^+$ ion; one trimethylstannyl anion coordinates via a K–Sn interaction, and the second coordinates via a K–$H_3C$ interaction. Simulations of the mechanochemical properties (compliance constants) applying approximated density functional theory revealed that both interactions are very soft and are of comparable strength. Moreover, according to our gas phase simulations the unsymmetrically coordinated $[(Me_2SnCH_3)K(18\text{-}C\text{-}6)SnMe_3]^-$ is indeed thermodynamically favored over both possible symmetrical isomers with either K–Sn or K–$H_3C$ coordination. Furthermore, the existence of multiple species due to the two coordination modes and aggregates of $[K(18\text{-}C\text{-}6)SnMe_3]$ in solution is suggested by NMR spectroscopic studies using $^1H$, NOESY/ROESY, and $^1H$ pulsed field gradient diffusion experiments.

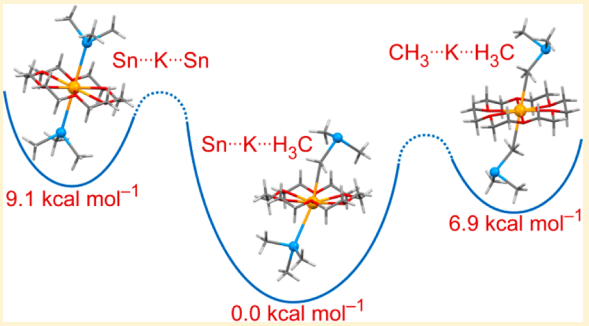


## INTRODUCTION

Stannyl (earth) alkaline metal complexes are established reagents in synthetic chemistry.[1] Structural investigations have mainly been performed on triaryl derivatives, and less is known on the trialkyl derivatives.[2,3,4a] To the best of our knowledge, only two crystal structures of potassium trialkylstannyls $[K(\eta^6\text{-}PhMe)_3Sn(CH_2{}^tBu)_3]$ and $[K(THF)_3Sn{}^tBu_3]$ have been reported.[3]

We recently synthesized a series of compounds of the type $[K(18\text{-}C\text{-}6)EPh_3]$ with E = C, Si, Ge, Sn, and Pb by alkoxide-induced cleavage of B–E bonds. In agreement with earlier reports, their solid state structures exhibit, for E = Sn and Pb, aryl–K interactions as the dominant structural motif.[2a,4] This reflects the strength of aryl–potassium interactions that can be competitive with K–dipole interactions as well as the weak donor capabilities of E in $[Ph_3Sn]^-$ and $[Ph_3Pb]^-$, respectively.[5] Furthermore, the scope of the alkoxide-induced B–E bond cleavage was investigated in some detail, being of relevance to the emerging field of Lewis base-promoted silyl-transfer reactions.[4b,6]

In the present work the scope of the Lewis base-induced B–E bond cleavage is further extended to the synthesis of trimethylstannyl potassium complexes, and the solid-state structural chemistry of those complexes is studied. Of particular interest is the structural impact of auxiliary neutral ligands at the potassium atom, with respect to an unprecedented $CH_3$–K coordination mode of the trimethylstannyl anion. The structure in solution as well as the nature of this coordination mode and the mechanochemical properties were further investigated by a combination of NMR spectroscopic techniques (NOESY, ROESY, and pulsed field gradient (PFG) diffusion experiments) and computational simulations.

## EXPERIMENTAL SECTION

**General Considerations.** ($^i$PrEn)BBr and $[K(18\text{-}C\text{-}6)O{}^tBu]$ were prepared according to literature procedures.[4a,7] All other compounds were commercially available and used as received. All solvents were

**Received:** January 10, 2014
**Published:** April 15, 2014

 © 2014 American Chemical Society  dx.doi.org/10.1021/ic500065s | Inorg. Chem. 2014, 53, 4400–4410

dried using MBraun solvent purification systems, deoxygenated using the freeze−pump−thaw method, and stored under purified nitrogen. All manipulations were performed using standard Schlenk techniques under an atmosphere of purified nitrogen or in a nitrogen-filled glovebox (MBraun). NMR spectra were recorded on Bruker Avance II 300, Bruker Avance 400, or Bruker DRX 400 spectrometers. Air-sensitive samples were generally measured in flame-sealed NMR tubes, while for short time measurements NMR tubes equipped with screw caps (Wilmad) were also employed. Chemical shifts ($\delta$) are given in ppm, using the residual resonance signal of the solvents ($C_6D_6$, Eurisotop, 99.5% deuteration; PhMe-$d_8$, Eurisotop, 99.5% deuteration; tetrahydrofuran (THF)-$d_8$, Eurisotop, 99.5% deuteration; all dried over potassium/benzophenone and degassed) as internal reference ($C_6D_6$: $^1$H NMR: 7.16 ppm, $^{13}$C NMR: 128.06 ppm; PhMe-$d_8$: $^1$H NMR: 2.08 ppm, $^{13}$C NMR: 20.43 ppm; THF-$d_8$: $^1$H NMR: 1.72 ppm, $^{13}$C NMR: 25.31 ppm).[8] $^{11}$B and $^{119}$Sn chemical shifts are reported relative to external $BF_3{\cdot}Et_2O$ and $SnMe_4$, respectively. $^{119}$Sn NMR spectra were recorded employing direct detection and composite pulse decoupling (inverse gated decoupling for **1** and **4**). $^{11}$B NMR spectra were processed applying a back linear prediction to suppress the broad background signal due to the borosilicate glass of the NMR tube and an exponential window function with the line-broadening parameter set to 10 Hz; the spectra were carefully evaluated to ensure that no genuinely broad signals of the sample were suppressed. $^1$H−$^1$H NOESY, ROESY, and $^1$H PFG diffusion measurements were performed on a Bruker DRX 400 spectrometer equipped with a 5 mm BBFO z-gradient probe, with a maximum gradient strength of 53.5 G/cm. Samples of a concentration of 1.4 mg/mL of complex **2** containing a trace of tetramethylsilane (TMS) as internal reference were used. Mixing time for NOESY and ROESY was 3 s and 300 ms, respectively.[9] For PFG diffusion experiments, pulse sequence with double stimulated echo (DSE) was used.[10a] The shape of the gradient was sinusoidal, with lengths of 2 or 3 ms. The gradient strength was varied in nine increments from 5 to 95% of the gradient ramp created by the Bruker software DOSY. Diffusion delays from 30 to 80 ms were used. Thus, all diffusion measurements were performed in a pseudo-two-dimensional mode and processed with the Bruker software package t1/t2 application. For each measurement, 16 dummy scans and 16 to 64 scans were used, with relaxation delays of 3.5 s. Melting points (mp) were determined using a Büchi 530 apparatus in flame-sealed capillaries under nitrogen and are not corrected. Elemental analyses were performed using an Elementar vario Micro cube instrument at the Institut für Anorganische und Analytische Chemie of the Technische Universität Carolo-Wilhelmina zu Braunschweig. Electron ionization (EI) mass spectra were obtained employing a Finnigan MAT 95 XP spectrometer (70 eV).

*[($^i$PrEn)B−SnMe$_3$] (**1**).* $Me_3SnCl$ (1.72 g, 8.6 mmol, 1 equiv) in dry THF (40 mL) was added to granulated lithium (0.25 g, 36 mmol, 2 equiv) in dry THF (20 mL) at room temperature (RT) and stirred for 16 h. The pale green solution was removed from the excess lithium and cooled to −78 °C. After addition of ($^i$PrEn)B−Br (2.00 g, 8.6 mmol, 1 equiv) in *n*-pentane (30 mL), the mixture was stirred for 16 h at RT. The solvent was removed *in vacuo*, and the gray residue was extracted with dry *n*-pentane (3 × 20 mL). After filtration of the combined extracts, the solvent was removed *in vacuo*, followed by bulb-to-bulb condensation ($2 \times 10^{-2}$ mbar). ($^i$PrEn)B−$SnMe_3$ (**1**) was obtained as a colorless liquid (2.61 g, 8.2 mmol, 95%). $^1$H NMR (400 MHz, $C_6D_6$, RT): $\delta$ 3.72 (sept., $^3J_{HH}$ = 7 Hz, 2 H, C*H*$(CH_3)_2$), 3.04 (s, 4 H, $CH_2$), 1.03 (d, $J_{HH}$ = 7 Hz, 12 H, CH(C*H*$_3)_2$), 0.30 (s, $^2J_{HSn}$ = 45, 47 Hz (satellites), 9 H, $Sn(CH_3)_3$). $^{13}$C{$^1$H} NMR (100 MHz, $C_6D_6$, RT): $\delta$ 47.7 (s, $^3J_{CSn}$ = 14 Hz (satellites), *C*H$(CH_3)_2$), 42.4 (s, $^3J_{CSn}$ = 44 Hz (satellites), $CH_2$), 22.4 (CH(*C*H$_3)_2$), −10.5 (s, $^1J_{CSn}$ = 255, 262 Hz (satellites), $Sn(CH_3)_3$). $^{11}$B{$^1$H} NMR (96 MHz, $C_6D_6$, RT): $\delta$ 35.9 (s, $^1J_{BSn}$ = 910 Hz (satellites), $\Delta w_{1/2}$ = 117 Hz). $^{119}$Sn{$^1$H} NMR (149 MHz, $C_6D_6$, RT): $\delta$ −152.2 (q, $^1J_{BSn}$ = 922 Hz, $\Delta w_{1/2}$ = 150 Hz). Mass spectroscopy (MS) (EI): 318 $[M]^+$, 303 $[M-CH_3]^+$, 153 $[M-SnMe_3]^+$. Anal. Calcd for $C_{11}H_{27}BN_2Sn$: C, 41.70; H, 8.59; N, 8.84. Found: C, 41.69; H, 8.53; N, 8.78%.

*[($^i$PrEn)B−O$^t$Bu].* ($^i$PrEn)B−Br (205 mg, 0.88 mmol, 1 equiv) in *n*-pentane (15 mL) was cooled to 0 °C, and a solution of KO$^t$Bu (103 mg, 0.92 mmol, 1.05 equiv) in THF (6 mL) was added. After it was stirred for 1 h at RT, the mixture was filtered over a plug of Celite, and the solvent was removed *in vacuo*. ($^i$PrEn)B−O$^t$Bu was obtained as a colorless liquid (80 mg, 0.35 mmol, 39%). $^1$H NMR (300 MHz, $C_6D_6$, RT): $\delta$ 3.77 (sept., $^3J_{HH}$ = 7 Hz, 2 H, C*H*$(CH_3)_2$), 2.98 (s, 4 H, $CH_2$), 1.35 (s, 9 H, OC$(CH_3)_3$), 1.06 (d, $^3J_{HH}$ = 7 Hz, 12 H, CH(C*H*$_3)_2$). $^{13}$C{$^1$H} NMR (75 MHz, $C_6D_6$, RT): $\delta$ 72.3 (O*C*$(CH_3)_3$), 43.8 (*C*H$(CH_3)_2$), 39.4 ($CH_2$), 31.8 (OC(*C*H$_3)_3$), 21.7 (CH(*C*H$_3)_2$). $^{11}$B{$^1$H} NMR (96 MHz, $C_6D_6$, RT): $\delta$ 24.3 ($\Delta w_{1/2}$ = 101 Hz). MS (EI): 226 (M), 153 ($[M-O^tBu]^+$). High-resolution mass spectrometry (HRMS) (EI): Calcd for $C_{12}H_{27}BN_2O$ ($M^+$): 226.221 87; found: 226.221 37.

*[K(18-C-6)SnMe$_3$] (**2**).* In a nitrogen-filled glovebox, [K(18-C-6)O$^t$Bu] (59 mg, 0.16 mmol, 1 equiv) and compound **1** (50 mg, 0.16 mmol, 1 equiv) were mixed in dry toluene (2 mL) and kept at RT for 10 min. After 6 h at −25 °C, the solvent was decanted, and the residue was washed with dry *n*-pentane and dried *in vacuo* to give 54 mg (0.12 mmol, 75%) of a microcrystalline powder. X-ray quality single crystals of **2** were obtained as described above but performing the crystallization at RT (CCDC 975919). $^1$H NMR (400 MHz, THF-$d_8$, RT): $\delta$ 3.62 (s, $OCH_2$), −0.48 (s, $^2J_{HSn}$ = 17 Hz (satellites), $Sn(CH_3)_3$). $^{13}$C{$^1$H} NMR (100 MHz, THF-$d_8$, RT): $\delta$ 71.1 ($OCH_2$), 0.2 (s, satellites not resolved, $Sn(CH_3)_3$). $^{119}$Sn{$^1$H} NMR (149 MHz, THF-$d_8$, RT): $\delta$ −164.9. $^1$H NMR (400 MHz, THF-$d_8$, 193 K): $\delta$ 3.63 (s, $OCH_2$), −0.55 (s, $^2J_{HSn}$ = 18 Hz (satellites), $Sn(CH_3)_3$). $^{13}$C{$^1$H} NMR (100 MHz, THF-$d_8$, 193 K): $\delta$ 71.1 ($OCH_2$), 0.4 ($Sn(CH_3)_3$, $^1J_{CSn}$ = 240, 251 Hz (satellites)). $^{119}$Sn{$^1$H} NMR (149 MHz, THF-$d_8$, 193 K): $\delta$ −168.0. $^1$H NMR (400 MHz, PhMe-$d_8$, RT): $\delta$ 3.25 (s, $OCH_2$), 0.54 (s, $^2J_{HSn}$ = 12 Hz (satellites), $Sn(CH_3)_3$). Only major peaks are given; see main text. mp > 160° (decomposition). Anal. Calcd for $C_{15}H_{33}O_6KSn$: C, 38.56; H, 7.12. Found: C, 38.32; H, 7.13%.

*[K(18-C-6)(THF)$_2$][K(18-C-6)(SnMe$_3$)$_2$] [**2**(THF)$_2$]$_2$.* X-ray quality single crystals were obtained by recrystallization of complex **2** from THF layered with *n*-pentane at −20 °C (CCDC 975920). Alternatively, (**2**(THF)$_2$)$_2$ was obtained following the protocol for **2** but using THF as solvent and crystallization under addition of *n*-pentane at −25 °C in 31% yield. Anal. Calcd for $C_{38}H_{82}O_{14}K_2Sn_2$: C, 42.31; H, 7.66. Found: C, 42.50; H, 7.58%.

*[K(TMEDA)$_2$SnMe$_3$] (**3**).* In a nitrogen-filled glovebox KO$^t$Bu (11 mg, 0.10 mmol, 1 equiv) was dissolved in a THF/TMEDA mixture (1 mL/0.5 mL) and added to compound **1** (31 mg, 0.10 mmol, 1 equiv). After 30 min the mixture was layered with *n*-pentane (4 mL) and cooled to −40 °C. After 40 h the product had separated as colorless crystals suitable for X-ray diffraction (CCDC 975921). The supernatant solution was decanted; the precipitate was washed with dry *n*-pentane (3 × 2 mL) and dried carefully in a stream of nitrogen (approximately 24 mg, 55 $\mu$mol, 56%). Drying of the product *in vacuo* results, according to elemental and NMR analysis, in the partial loss of TMEDA. $^1$H NMR (300 MHz, THF-$d_8$, RT): $\delta$ 2.29 (s, 8 H, ($CH_2N(CH_3)_2)_2$), 2.14 (s, 24 H, ($CH_2N(CH_3)_2)_2$), −0.43 (s, $^2J_{HSn}$ = 12 Hz (satellites), 9 H, $Sn(CH_3)_3$). $^{13}$C{$^1$H} NMR (75 MHz, THF-$d_8$, RT): $\delta$ 58.9 (($CH_2N(CH_3)_2)_2$), 46.2 (($CH_2N(CH_3)_2)_2$), −1.5 ($Sn(CH_3)_3$, $^1J_{CSn}$ = 208, 198 Hz (satellites)). Anal. Calcd for $C_3H_9KSn(C_6H_{16}N_2)_{1/4}$: C, 23.30; H, 5.65; N, 3.02. Found: C, 22.97; H, 5.32; N, 2.85% (*vide supra*).

*[K(12-C-4)$_2$][SnMe$_3$] (**4**).* In a nitrogen-filled glovebox, KO$^t$Bu (16 mg, 0.14 $\mu$mol, 1 equiv) was dissolved in dry THF/12-C-4 (1 mL/0.2 mL), and compound **1** (46 mg, 0.15 $\mu$mol, 1.1 equiv) was added. After 1 h *n*-pentane was added until turbid, and the mixture was cooled to −20 °C. After 20 h, complex **4** had separated as colorless crystals suitable for X-ray diffraction (CCDC 975922). The product was isolated after decanting the supernatant solution, washing the precipitate with dry *n*-pentane (2 × 2 mL) and drying *in vacuo* (14 mg, 0.025 mmol, 18%). Compound **4** decomposes slightly upon drying: THF solutions of analytically pure **4** repeatedly contained, according to $^1$H NMR spectroscopy, a small excess of the 12-C-4 compared to $SnMe_3$ groups (molar ratio typically 2.4:1); it was also noted that the material did not dissolve completely in THF. This may suggest the partial formation of an insoluble, polymeric material under


dx.doi.org/10.1021/ic500065s | Inorg. Chem. 2014, 53, 4400−4410

Table 1. Crystallographic Data Collection Parameters for Complexes 2, 3, 4, and $[2(THF)]_2$

| compound | 2 | 3 | 4[a] | $[2(THF)]_2$ |
|---|---|---|---|---|
| chemical formula | $C_{15}H_{33}KO_6Sn$ | $C_{15}H_{41}KN_4Sn$ | $C_{19}H_{41}KO_8Sn$ | $C_{38}H_{82}K_2O_{14}Sn_2$ |
| crystallization conditions | PhMe | THF/TMEDA/*n*-pentane | THF/12-C-4/*n*-pentane | THF/*n*-pentane |
| | RT | −40 °C | −20 °C | −20 °C |
| formula mass (g mol$^{-1}$) | 467.20 | 435.31 | 555.31 | 1078.62 |
| crystal dimensions (mm$^3$) | 0.11 × 0.16 × 0.18 | 0.36 × 0.04 × 0.04 | 0.41 × 0.18 × 0.13 | 0.48 × 0.32 × 0.26 |
| crystal shape, crystal color | cuboid, colorless | needle, colorless | column, colorless | fragment, colorless |
| crystal system, space group (no.) | triclinic, $P\bar{1}$ (2) | monoclinic, $P2_1/c$ (14) | monoclinic, $P2_1/m$ (11) | triclinic, $P\bar{1}$ (2) |
| $Z$, $Z'$ | 2, 1 | 8, 2 | 2, 1/2 | 2, 1 |
| $a$ (Å) | 8.8884(9) | 14.652(1) | 7.622(1) | 9.4936(2) |
| $b$ (Å) | 8.8903(8) | 22.345(2) | 21.232(4) | 16.6351(3) |
| $c$ (Å) | 15.036(1) | 14.464(1) | 8.148(1) | 17.0426(3) |
| $\alpha$ (deg) | 80.612(7) | 90 | 90 | 94.374(2) |
| $\beta$ (deg) | 81.612(7) | 99.960(5) | 99.08(2) | 98.663(2) |
| $\gamma$ (deg) | 67.214(8) | 90 | 90 | 102.959(2) |
| volume (Å$^3$) | 1076.3(2) | 4664.1(6) | 1302.0(4) | 2576.04(8) |
| $D_{calcd}$ (Mg m$^{-3}$) | 1.442 | 1.240 | 1.416 | 1.391 |
| T (K) | 100(2) | 100(2) | 100(2) | 100(2) |
| radiation, $\lambda$ (Å) | Cu K$\alpha$, 1.541 84 | Cu K$\alpha$, 1.541 84 | Mo K$\alpha$, 0.710 73 | Mo K$\alpha$, 0.710 73 |
| $\mu$ (mm$^{-1}$) | 11.372 | 10.303 | 1.177 | 1.185 |
| refl. coll./indep./obs. ($I > 2\sigma(I)$) | 16 780/4418/4300 | 69 064/8848/5692 | 5732/5732/3720 | 162 116/14 546/12 552 |
| no. of variables/restraints | 244/3 | 452/0 | 251/120 | 532/0 |
| $\theta$ range (deg) | 5.42 < $\theta$ < 75.00 | 3.65 < $\theta$ < 69.99 | 2.53 < $\theta$ < 26.99 | 2.23 < $\theta$ < 29.75 |
| GOF on $F^2$ | 1.056 | 1.085 | 0.946 | 1.051 |
| $R_{int}$ | 0.0363 | 0.1010 | n/a[a] | 0.0384 |
| $R_1$ [$I > 2\sigma(I)$][b] | 0.0262 | 0.0524 | 0.0641 | 0.0229 |
| $wR_2$ (all data)[c] | 0.0678 | 0.1584 | 0.1430 | 0.0523 |
| weighting parameters $a$, $b$ | 0.0400, 0.8738 | 0.0627, 4.339 | 0.0759, 0.0000 | 0.0208, 1.2008 |
| largest diff peak/hole (Å$^{-3}$) | 0.827/−0.947 | 0.953/−1.250 | 2.752/−0.790 | 0.662/−0.899 |
| CCDC no. | 975919 | 975921 | 975922 | 975920 |

[a]The crystal is a nonmerohedral twin, hence no $R_{int}$ can be calculated, see also reference 14. [b]$R_1 = \Sigma||F_o| - |F_c||/\Sigma|F_o|$. [c]$wR_2 = (\Sigma[w(F_o^2 - F_c^2)]/\Sigma[F_o^4])^{1/2}$, where $w = 1/[\sigma^2(F_o^2) + (aP)^2 + (bP)]$ with $P = (F_o^2 + 2F_c^2)/3$.

release of 12-C-4. $^1$H NMR (400 MHz, THF-$d_8$, RT): $\delta$ 3.65 (s, 32 H, $OCH_2$ (*vide supra*)), −0.43 (s, $^2J_{HSn}$ = 12 Hz (satellites), 9 H, $Sn(CH_3)_3$). $^{13}C\{^1H\}$ NMR (100 MHz, THF-$d_8$, RT): $\delta$ 69.5 ($OCH_2$), −0.4 (s, $^1J_{CSn}$ = 222 Hz (satellites)). $^{119}Sn\{^1H\}$ NMR (149 MHz, THF-$d_8$, RT): $\delta$ −168.1. Anal. Calcd for $C_{19}H_{41}O_8KSn$: C, 41.09; H, 7.44. Found: C, 40.95; H, 7.11%.

**X-ray Crystallography.** All crystals were transferred into inert perfluoroether oil inside a nitrogen-filled glovebox; outside of the glovebox, they were rapidly mounted on top of a human hair and transferred to the cold nitrogen gas stream of the diffractometer.[11a] The data were either collected on an Oxford Diffraction Xcalibur E instrument using monochromated Mo K$\alpha$ radiation or on an Oxford Diffraction Nova A instrument, using mirror-focused Cu K$\alpha$ radiation. Additional data collection parameters are indicated in Table 1. The data were integrated, and an empirical absorption correction was performed employing the CrysAlisPro software.[11b] All structures were solved by employing SHELXS-97 or -86 and refined anisotropically for all non-hydrogen atoms by full-matrix least-squares on all $F^2$ using SHELXL-97.[11c] Hydrogen atoms were generally refined employing a riding model. For certain methyl groups in **2** (C1 to C3) and $(2(THF))_2$ (C16) the hydrogen atoms were refined freely. In the case of **2** (C3) similarity restraints were employed on the H−C−H angles. During refinement and analysis of the crystallographic data, the programs WinGX, PLATON, Mercury, and Diamond were used.[11d−g] Thermal ellipsoids are drawn at the 50% probability level. Only selected hydrogen atoms are shown. Symmetry-equivalent atoms are denoted by a prime.

## RESULTS AND DISCUSSION

**Synthesis.** The stannylborane ($^i$PrEn)B−$SnMe_3$ (**1**) ($^i$PrEn = $(^i PrN)_2C_2H_4$) was synthesized following an established route from the respective bromoborane and $LiSnMe_3$.[4a,12] The stannylborane **1** was reacted with the crown ether potassium *tert*-butoxide complex [K(18-C-6)O$^t$Bu], and the reaction was monitored by *in situ* $^{11}$B NMR spectroscopy (Figure 1).[7]

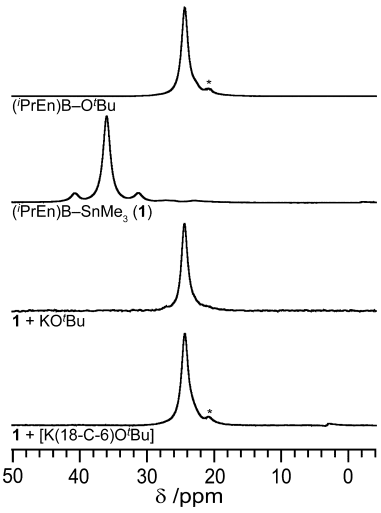


**Figure 1.** Details of the *in situ* $^{11}B\{^1H\}$ NMR spectra of reaction mixtures of compound **1** with [K(18-C-6)O$^t$Bu] (in $C_6D_6$, after 30 min at RT) and compound **1** with KO$^t$Bu (in THF-$d_8$, after 30 min at RT). Complex **1** and ($^i$PrEn)B−O$^t$Bu in $C_6D_6$ are shown for comparison (96.3 MHz, RT, * = impurity).


dx.doi.org/10.1021/ic500065s | Inorg. Chem. 2014, 53, 4400−4410

During the conversion a new signal at 24.3 ppm appeared, which is, according to comparison with an authentic sample, indicative of the formation of ($^i$PrEn)B−O$^t$Bu. The formation of this boric acid derivative as the only boron-containing species is suggestive of B−Sn bond cleavage and concomitant formation of the trimethylstannyl anion.[4,6e] However, this is contrary to the related reaction of pinB−SiMe$_2$Ph (pin = OCMe$_2$CMe$_2$O), leading ultimately to the formation of [pinB(SiMe$_2$Ph)$_2$]$^-$ as a Lewis acid/base adduct of the respective silyl anion with the parent silylborane.[4b] This different outcome of the reaction may be rationalized with the reduced Lewis acidity of the ($^i$PrEn)B moiety compared to the pinB moiety and the reduced Lewis basicity of the [SnMe$_3$]$^-$ compared to [SiMe$_2$Ph]$^-$. Indeed, the stannyl potassium complex [K(18-C-6)SnMe$_3$] (**2**) was isolated from the reaction of **1** with [K(18-C-6)O$^t$Bu] in PhMe in 75% yield as a colorless microcrystalline solid under optimized conditions (Scheme 1).

**Scheme 1. Products of the Heterolytic B−Sn Cleavage of Complex 1 with $^t$BuO$^-$ under Different Conditions**

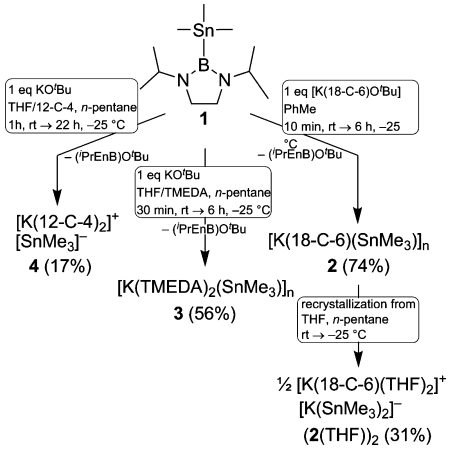


The formation of ($^i$PrEn)B−O$^t$Bu in the reaction of compound **1** with KO$^t$Bu in THF-$d_8$ is again indicative of B−Sn bond cleavage and, hence, suggests the formation of a stannyl anion also under these conditions (Figure 1). However, no uniform materials could be isolated from reactions in THF, but the reaction in a THF/TMEDA (2:1) mixture led to the isolation of [K(TMEDA)$_2$SnMe$_3$] (**3**) as a crystalline material (Scheme 1).[13] Similarly, the reaction of **1** with KO$^t$Bu in a THF/12-C-4 mixture (5:1) led to the isolation of [K(12-C-4)$_2$][SnMe$_3$] (**4**) as a crystalline material suitable for an X-ray structure determination (Scheme 1).

**Solid-State Structures.** Single crystals of complex **2**, suitable for an X-ray structure determination, crystallized from the reaction mixture in PhMe at ambient temperature. Compound **2** crystallizes in large colorless, well-developed cuboids in the triclinic space group type $P\bar{1}$ with one unit of **2** in the asymmetric unit. The individual units of **2** form infinite chains [K(18-C-6)SnMe$_3$]$_n$ parallel to the *b*-axis consisting of alternating units of [K(18-C-6)]$^+$ and [SnMe$_3$]$^-$ (Figure 2). The K−Sn distance (Table 2) is well below the sum of the van der Waals radii (4.92 Å).[15a] In fact, the K−Sn distance is comparable to the value found for [K($\eta^6$-PhMe)$_3$Sn(CH$_2$$^t$Bu)$_3$] (3.548(3) Å), thus far the only structurally characterized potassium trialkylstannylide.[3a] The longer (by 0.09 Å) K−Sn distance in **2** may be attributed to the changed coordination

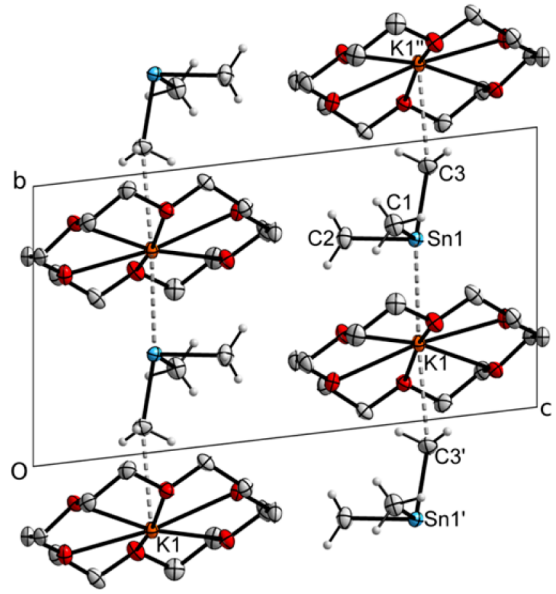


**Figure 2.** Detail of the solid-state structure of complex **2**, viewed along the *a*-axis. Only methyl hydrogen atoms are shown.

environment at the potassium atom, rather than being indicative of a weaker K−Sn interaction. It should also be stated that the "intramolecular" K1−C1distance is significantly shorter than the sum of the respective van der Waals radii (4.45 Å), suggesting an interaction of K1 with both Sn1 and the C1 methyl group, rather than a pure Sn1−K1 coordination.[15a]

However, the most interesting feature of this structure is the bidentate coordination mode of the trimethylstannyl anion coordinating via the Sn atom and a H$_3$C moiety to a K atom. This structural motif is reflected in the short C3′−K1 (or C3−K1″) distance (Table 2), which is 1.27 Å smaller than the sum of the van der Waals radii of 4.45 Å; hence, a substantial K−H$_3$C interaction can be assumed.[15,16] The atom K1 is situated slightly out of the O$_6$ mean plane toward atom Sn1 (Table 2, Figure 2), and the coordination environment of K1 may be described as a distorted hexagonal bipyramid.

Similarly short K−H$_3$C interactions have occasionally been reported, but to the best of our knowledge they have not been analyzed in greater detail.[17] However, the related compounds [K(18-C-6)E(SiMe$_3$)$_3$] (E = Si, Ge) exhibit similar chain structures as observed for complex **2** with comparably small K−H$_3$C distances in the solid state (3.24−3.28 Å).[18] Moreover, a similar structural motif, the *inv* coordination of H$_3$Si$^-$ to a potassium and sodium cation, respectively, has been described and analyzed in some detail.[19]

It has to be emphasized that all structural data within the triphenylstannyl moiety for complex **2** are consistent with the presence of a trimethylstannyl anion and that no indications are found for an isomeric species [Me$_2$SnH−CH$_2$]$^-$, which could also explain the structural peculiarities of **2**. In particular, have all methyl hydrogen atoms during the X-ray structure determination of **2** been localized and refined freely employing only geometry restraints on the H−C−H angles of the C3 methyl group.[20]

The compound [K(TMEDA)$_2$SnMe$_3$] (**3**) was obtained by performing the B−Sn cleavage reaction in a THF/TMEDA mixture followed by crystallization under addition of *n*-pentane. Compound **3** crystallizes with two formula units in the asymmetric unit in the monoclinic space group type $P2_1/c$.


dx.doi.org/10.1021/ic500065s | Inorg. Chem. 2014, 53, 4400−4410

**Table 2. Selected Bond Lengths and Angles for Complexes 2, 3, 4, and $[2(THF)]_2$**

| compound | 2[a] | 3[a,b] | 4[a] | $[2(THF)]_2$[a] |
|---|---|---|---|---|
| K–Sn (Å) | 3.636(1) (K1, Sn1) | 3.693(2) (K1, Sn1) | 6.700(3) (K1, Sn1) | 3.6788(3) (K1, Sn1) |
| | 5.354(1) (K1, Sn1′) | 3.697(2) (K2, Sn2) | 6.920(3) (K1′, Sn1) | 5.4033(3) (K1, Sn2) |
| K–$H_3C$–$Sn(CH_3)_2$ (Å) | 3.181(3) (K1, C3′) | 3.700(8) (K1′, C18) | 6.869(5) (K1, C2) | 3.237(2) (K1, C16) |
| | 3.539(3) (K1, C1) | 3.668(6) (K2, C3) | 6.890(6) (K1, C1) | 5.097(2) (K1, C15) |
| K–$H_3C$–Sn (deg) | 164.7(1) (Sn1′, C3′, Sn1) | 145.3(3) (K1), 147.1(3) (K2) | | 161.41(8) (Sn2, C16, K1) |
| $CH_3$–K–Sn (deg) (K) | 165.03(6) (K1) | 168.1(1) (K1), 169.1(1) (K2) | | 172.25(3) (K1) |
| Sn–$CH_3$ (Å) | 2.234(3) (Sn1, C1) | 2.23–2.25 (Sn1, C1–3) | 2.225(4) (Sn1, C1) | 2.22–2.24 (Sn1, C13–15) |
| | 2.225(3) (Sn1, C2) | 2.21–2.22 (Sn2, C16–18) | 2.225(4) (Sn1, C1′) | 2.22–2.24 (Sn2, C16–18) |
| | 2.220(3) (Sn1, C3) | | 2.216(7) (Sn1, C2) | |
| $H_3C$–Sn–$CH_3$ (deg) | 94.0(1) (C1, Sn1, C2) | 88.8–100.8 (Sn1, C1–3) | 92.6(2) (C1, Sn1, C2) | 91.8–94.8 (Sn1, C13–15) |
| | 93.4(1) (C2, Sn1, C3) | 92.5–96.7 (Sn2, C16–18) | 92.6(2) (C1′, Sn1, C2) | 89.7–95.0 (Sn1, C16–18) |
| | 93.5(1) (C3, Sn1, C1) | | 90.8(3) (C1, Sn1, C1′) | |
| $\Delta(K–L_n)$[c] (Å) | 0.264(1) | 0.308(2) (K2), 0.310(2) (K1) | 1.876(3), 1.882(3) | 0.3035(3) (K1) |

[a]A prime denotes symmetry-equivalent atoms as given in the respective figure. [b]Disordered structure; data of the major site with the occupancy (0.6959(9)).[21] [c]Deviation of the K atom from the auxiliary ligand atoms mean plane.

The solid-state structure of this compound is closely related to that of **2** and comprises polymeric chains of $[K(TMEDA)_2SnMe_3]_n$ parallel to the [101] direction. These chains consist of alternating units of $[K(TMEDA)_2]^+$ and $[SnMe_3]^-$. As found for **2**, the trimethylstannyl anion bridges two $[K(TMEDA)_2]^+$ moieties by coordination via the Sn atom and one methyl group. Each individual $[K(TMEDA)_2SnMe_3]_n$ chain consists of two crystallographically independent $[K(TMEDA)_2]^+$ and $[SnMe_3]^-$ moieties (K1/Sn1 and K2/Sn2, respectively; Figure 3). Within each chain the $[SnMe_3]^-$ moieties are seriously disordered on a noncrystallographic 2-fold axis parallel to the *b*-axis coinciding with the crystallographic $2_1$ screw axis (ratio of occupancy 7:3).[21] The data obtained confirm a similar chain structure as in **2** and especially the presence of the unusual K–$H_3C$ coordination motif for **3** (Table 2). A detailed discussion of the respective geometrical parameters is prohibited by the compromised quality of the structure of **3** because of correlation effects due to the substantial disorder present.

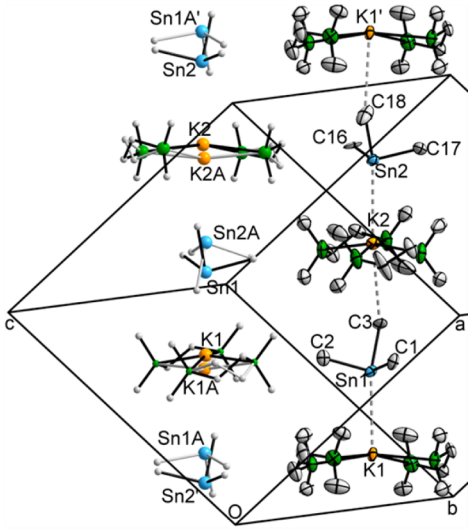


**Figure 3.** Detail of the solid-state structure of complex **3**. The disorder is displayed within one $[K(TMEDA)_2SnMe_3]_n$ chain only (left). The atoms in this chain are displayed as spheres with an arbitrary radius.

The compound $[K(12\text{-}C\text{-}4)_2][SnMe_3]$ (**4**) was obtained from the reaction of **1** with $KO^tBu$ in THF/12-C-4 followed by crystallization under addition of *n*-pentane. The solid-state structure is significantly different from those of **2** and **3** (and also of $[2(THF)]_2$, *vide infra*). Here, separated ions of $[K(12\text{-}C\text{-}4)_2]^+$ and $[SnMe_3]^-$ are found, and no directed interactions between both ions are obvious as suggested by the large shortest K–Sn and K–$H_3CSnMe_2$ distances (Table 2, Figure 4). However, the Sn–$CH_3$ distances and $H_3C$–Sn–$CH_3$ angles are comparable to those found in **2**, **3**, and $[2(THF)]_2$. Within the unit cell in the space group type $P2_1/m$ the $[K(12\text{-}C\text{-}4)_2]^+$ moieties are situated on inversion centers along a 2-fold screw axis. However, the entire moiety $[K(12\text{-}C\text{-}4)_2]^+$ is disordered as the potassium atom is situated 0.3 Å off the center of inversion.

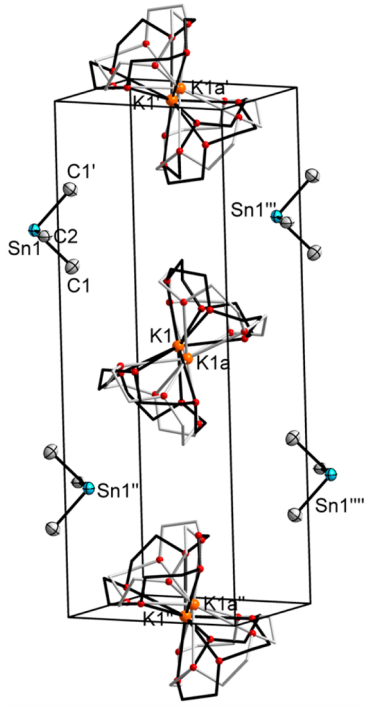


**Figure 4.** Detail of the solid-state structure of **4**. The disorder in the 12-C-4 moiety is displayed with gray bonds; only $Sn(CH_3)_3$ moieties are drawn with thermal ellipsoids at the 50% probability level; other atoms are drawn as spheres with arbitrary radius.


dx.doi.org/10.1021/ic500065s | Inorg. Chem. 2014, 53, 4400–4410

In contrast the tin and one carbon atom of the $[SnMe_3]^-$ moiety is situated on a mirror plane perpendicular to a 2-fold screw axis.[14]

The formation of separated ion pairs upon change from $[K(18\text{-}C\text{-}6)]^+$ to $[K(12\text{-}C\text{-}4)_2]^+$ as counterions is not surprising nor unprecedented and has been reported for related potassium complexes of $[E(SiMe_3)_3]^-$ (E = Si, Ge).[18]

Crystallization of **2** from a mixture of THF and *n*-pentane at −20 °C resulted in well-developed crystals in the triclinic space group type $P\bar{1}$ containing one molecule of cocrystallized THF per molecule **2**. Though the compound obtained can be formally described as $[\mathbf{2}(THF)]_2$, the presence of the donor solvent THF leads to a significant change in the connectivity: while complex **2** consists of $[K(18\text{-}C\text{-}6)SnMe_3]_n$ chains, $[\mathbf{2}(THF)]_2$ consists of the ion pair $[K(18\text{-}C\text{-}6)(THF)_2]^+[K(18\text{-}C\text{-}6)(SnMe_3)_2]^-$. However, in the structurally remarkable anion the $CH_3$−K−Sn coordination motif of the chain structure of **2** is preserved. The anion contains two different $SnMe_3$ moieties: one coordinating via the tin atom Sn1 to the potassium atom K1, while the other coordinates via the methyl group at atom C16 (Figure 5). Emphasizing the unsymmetrical

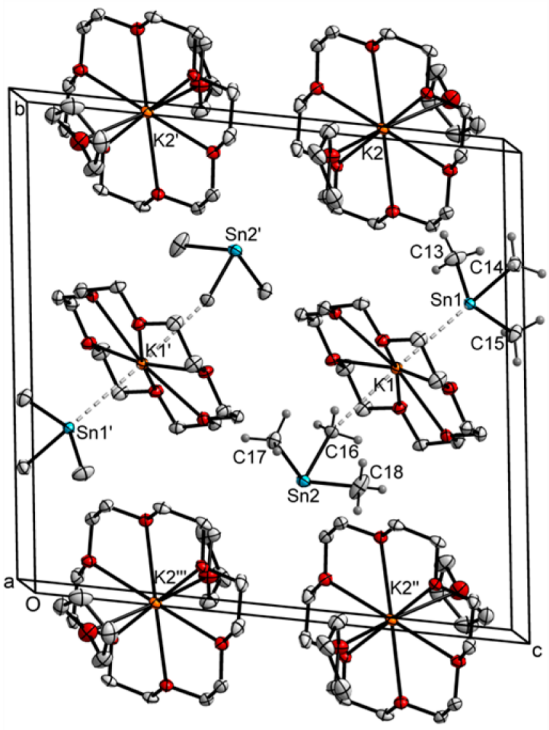


**Figure 5.** Detail of the solid-state structure of $[\mathbf{2}(THF)]_2$. Only selected methyl-group hydrogen atoms are shown; a disorder in a THF moiety is omitted for clarity.

coordination it may be written as $[(Me_2SnCH_3)K(18\text{-}C\text{-}6)SnMe_3]^-$. Hence, the formation of the ion pair $[K(18\text{-}C\text{-}6)(THF)_2]^+[K(18\text{-}C\text{-}6)(SnMe_3)_2]^-$ in $[\mathbf{2}(THF)]_2$ may be rationalized by coordination of every second $[K(18\text{-}C\text{-}6)]^+$ moiety within the structural motif found for complex **2** by two THF molecules, leaving the remaining $[(Me_2SnCH_3)K(18\text{-}C\text{-}6)SnMe_3]^-$ moieties intact (Figure 5). The structural parameters within the $[(Me_2SnCH_3)K(18\text{-}C\text{-}6)SnMe_3]^-$ moiety in $[\mathbf{2}(THF)]_2$ are very similar to the respective parameters in **2**; only a slight elongation of the K−Sn and K−$H_3C$ distances (K1−Sn1/K1−Sn1 and K1−$H_3C$/K1−C3′, respectively) is observed. The atom K1 is situated slightly out of the $O_6$ mean plane toward atom Sn1 within a distorted hexagonal bipyramid (Table 2, Figure 5), suggesting K−Sn and K−$H_3C$ interactions of comparable strength. Again it should be noted that in $[\mathbf{2}(THF)]_2$ the methyl hydrogen atoms at C16 were refined freely, giving no indication for the possible presence of an isomeric $[Me_2SnH{-}CH_2]^-$ species.

In conclusion, $CH_3$−K interactions are a common feature of the solid-state structures of the trimethylstannyl potassium complexes **2**, **3**, and most pronounced in $[\mathbf{2}(THF)]_2$. The formation of polymeric chains of $[K(L)SnMe_3]_n$ (L = 18-C-6, $TMEDA_2$) in the structures of **2** and **3** may well be driven by packing effects. In a simplified model the $[K(L)SnMe_3]$ moieties may be described as dipoles forming head-to-tail chains that minimize repulsion and optimize attractive dipole−dipole interactions within each $[K(L)SnMe_3]_n$ chain, resulting directly in the observed K−$H_3C$ interactions. Consistent with this picture are the adjacent parallel chains askew, leading also to optimized intercolumnar dipole−dipole interactions. Moreover, this simple rationalization is consistent with the observation of similar chain structures in other related compounds, which may be described as dipoles consisting of a $[K(18\text{-}C\text{-}6)]^+$ and an anionic moiety, for example, $[K(18\text{-}C\text{-}6)E(SiMe_3)_3]$ (E = Si, Ge).[17,18]

However, this simple picture is not valid for $[\mathbf{2}(THF)]_2$, consisting of the ion pair of $[K(18\text{-}C\text{-}6)(THF)_2]^+$ and the unsymmetrical $[(Me_2SnCH_3)K(18\text{-}C\text{-}6)SnMe_3]^-$. While the unsymmetrical $[(Me_2SnCH_3)K(18\text{-}C\text{-}6)SnMe_3]^-$ moiety may well be regarded as consisting of a $[K(18\text{-}C\text{-}6){-}SnMe_3]$ dipole and a trimethylstannyl anion, this provides no explanation for the unsymmetrical coordination of the potassium atom via a $CH_3$−K and a Sn−K interaction. Moreover, a clear difference to the related complexes $[K(18\text{-}C\text{-}6)E(SiMe_3)_3]$ (E = Si, Ge) is observed: the latter ones form polymeric chains similar to complex **2** (*vide supra*) upon crystallization in the presence of THF, and no ion pair formation is observed.[18] This emphasizes the peculiarity of $[\mathbf{2}(THF)]_2$ and justifies a more detailed analysis of the interactions present in $[\mathbf{2}(THF)]_2$.

**Molecular Statics Simulations.** To further elucidate the $CH_3$−K and Sn−K interactions, we performed a series of computer simulations at the approximated density functional (DF) level of theory on the three isomeric anions $[(Me_2SnCH_3)K(18\text{-}C\text{-}6)SnMe_3]^-$ (**I**, $CH_3$−K−Sn coordination), $[K(18\text{-}C\text{-}6)(H_3CSnMe_2)_2]^-$ (**II**, $CH_3$−K−$H_3C$ coordination), and $[K(18\text{-}C\text{-}6)(SnMe_3)_2]^-$ (**III**, Sn−K−Sn coordination) (Table 3). All molecular statics computations were based on the meta-hybrid functional M06-L, which includes empirical fitting parameters to describe dispersion forces, combined with a polarized triple-ζ basis set.[22a,22b] The element tin was described by an effective core potential.[22c] Energies and Cartesian force constants were computed with the Gaussian 09 set of programs, while all mechanochemical properties (compliance constants, relaxed force constants) were computed with our freely available Compliance code.[22d,e] Preliminary calculations showed that all three isomers are minima and exhibit no significant imaginary frequencies. Selected structural parameters and relative energies are given in Table 3.[20]

The computations were done in the gas phase to directly discriminate between crystal packing effects and intrinsic stabilization of the ion pairs. Because of our computations the unsymmetrical isomer **I** is indeed significantly stabilized in comparison with both symmetrical isomers **II** and **III** by 6.9 and 9.1 kcal/mol, respectively (Table 3). We can therefore


dx.doi.org/10.1021/ic500065s | Inorg. Chem. 2014, 53, 4400−4410

**Table 3. Selected Structural Data, Relative Energies, and Relaxed Force Constants *k* of the Calculated Isomeric Anions I, II, and III with Different Coordination Modes**

| isomer | I | II | III |
|---|---|---|---|
| coord. mode | (Sn−K−Me) | (Me−K−Me) | (Sn−K−Sn) |
| $\Delta E$ /kcal mol$^{-1}$ | 0.00 | 6.9 | 9.1 |
| K−Sn/Å | 3.66 | | 3.60, 3.60 |
| $k$/N cm$^{-1}$ | 0.18 | | 0.22, 0.22 |
| K−$H_3$C/Å | 3.16 | 3.13, 3.13 | |
| $k$/N cm$^{-1}$ | 0.17 | 0.16, 0.16 | |
| L−K−L′ (L,L′) | 160.9° (C, Sn) | 180.0° (C, C) | 180.0° (Sn, Sn) |
| K−$H_3$C−Sn | 153.2° | 145.8°, 145.8° | |

exclude crystal packing effects as the driving force for the observed Sn−K−Me coordination in the solid state. Moreover, the calculated gas-phase structure of this anion resembles the observed solid-state structure reasonably well (Tables 2 and 3, Figure 6). The small residual differences may indeed be due to packing effects in the solid state. All the structural distortions within the Sn−K−$H_3$C−Sn subunit are small and associated with weak interatomic forces (Table 3).

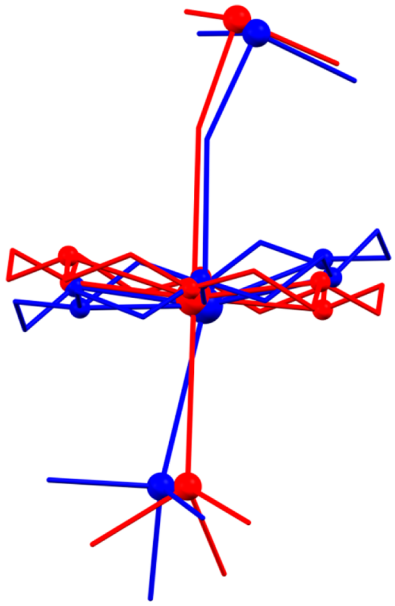

**Figure 6.** Overlay of the solid-state structure (red) and the calculated structure (blue) of the unsymmetrical species [($Me_2SnCH_3$)K(18-C-6)($SnMe_3$)]$^-$. Non-C atoms are drawn as spheres with arbitrary radius; H atoms omitted for clarity.

To (1) quantify these forces and (2) to get a feeling for the curvature of the relevant energy profiles, we simulated the mechanochemical properties of the anions applying the compliance constants method.[23] The description in terms of compliance constants allows a comparison of chemically different systems because, in contrast to normal mode force constants, they do not depend on the masses of the vibrating atoms and, most important, are independent of the chosen internal coordinate system. This is also true for soft interactions. Unfortunately, there are still some irritations about this topic in the literature.[24] In the following we are presenting relaxed force constants (unit: N/cm; the inverse of compliance constants) to facilitate the comparison with older literature values. While the unsymmetrical isomer **I** is thermodynamically clearly favored over the symmetrical isomers **II** and **III** the relaxed force constants (Table 3) for the K−Sn and K−$H_3$C interactions, respectively, show a different trend: focusing just on the sum of the local K−Sn and K−$H_3$C interactions, the unsymmetrical isomer (**I**) and the symmetrical isomer (**II**, Me−K−Me) depict more or less the same elasticity (0.16−0.17 N/cm), while for the symmetrical isomer (**III**), thermodynamically destabilized by 9.1 kcal/mol, the Sn−K−Sn interaction is significantly stronger (0.22 N/cm). Our calculated relaxed force constants both for the K−Sn and the K−$H_3$C contact are 1 order of magnitude lower than they are for a typical covalent bond but are comparable to other noncovalent interactions like, for example, H-bonds.[25] While this was to be expected for the K−$H_3$C interaction, it is quite surprising for the K−Sn bond and points to the inherent weakness of this contact. These results clearly suggest that the weak K−Sn and K−$H_3$C interactions are not solely causal for the thermodynamic stability but only for a subgroup of the large concert of noncovalent atom−atom contacts. Only the integral of all other (weak) interactions (e.g., with the periphery of the 18-C-6 moiety) is decisive for the overall stability of the anions. This intricacy of noncovalent interactions is a common feature in supramolecular chemistry and has consequences, for example, in the field of molecular recognition and drug design.[26]

To gain further insight into the mechanism of the potassium complex we compared the calculated relative energies for the association of the first and second [$SnMe_3$]$^-$ to the [K(18-C-6)]$^+$ unit to form **I** with respect to the K−Sn and K−$H_3$C coordination mode (Scheme 2). In the first association step the formation of the K−Sn coordinated isomer is favored by more than 5 kcal mol$^{-1}$ over the K−$H_3$C isomer. In contrast, in the second association step K−$H_3$C coordination is favored by the same energies over the K−Sn isomer. Hence, the mode of the

**Scheme 2. Association Energies for the Formation of Isomer I from [K(18-C-6)]$^+$ by Stepwise Addition of Two [$SnMe_3$]$^-$ Ions; Gas-Phase Calculations, Relative Energies in kcal mol$^{-1}$**

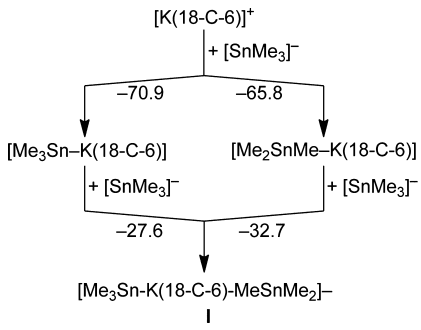



dx.doi.org/10.1021/ic500065s | Inorg. Chem. 2014, 53, 4400−4410

first coordination determines the mode of the second in a cooperative manner.

**NMR Investigation.** To gain a deeper insight into the solution-state structure and especially aggregation behavior in solution we performed a thorough NMR spectroscopic study on complex **2**. Thus, NOESY and ROESY spectra of **2** were recorded both in THF-$d_8$ and in toluene-$d_8$ (Tol-$d_8$) at 298 K. In THF-$d_8$ solution at a concentration of about 1.4 mg/mL the $^1$H spectrum shows one major peak accompanied by another six minor peaks for the $SnMe_3$ moieties. The major peak comprises about 70% of the intensity of these signals as a whole. At 298 K, the major peak was detected at −0.48 ppm, while the minor peaks were observed at 0.14, 0.06, 0.01, −0.03, −0.08, and −0.21 ppm. These assigned signals were verified by reading cross peaks in the NOESY spectrum (Figure 7).[20] For

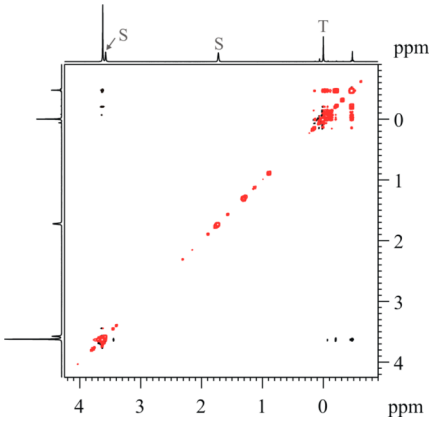


**Figure 7.** $^1$H−$^1$H NOESY NMR spectrum of complex **2** in THF-$d_8$ at 298 K. Mixing time 3 s. Cross peaks in black are due to NOE contact, while cross peaks in red are due to chemical exchange. The labels to the one-dimensional reference spectrum on top are S for solvent and T for TMS. See text for details.

the 18-C-6 signal, on the contrary, one sharp signal (line width of 2 Hz) at 3.62 ppm was observed at 298 K, while at 193 K two broad signals (line width 10 Hz) at 3.63 and 3.53 were observed, with an intensity ratio of 75:25%. As shown in Figure 7, three cross peaks due to positive NOE contacts are present between the 18-C-6 signal at 3.62 ppm and the signals of the $SnMe_3$ moieties at −0.08, −0.21, and −0.47 ppm, with relative NOE intensities of 4, 10, and 100%, respectively. The observation of three different NOE contact modes corresponds very well to the different coordination modes of $[SnMe_3]^-$ and to three structure motifs involving $[SnMe_3]^-$ observed in solid state, namely, $[K(18\text{-C-6})\text{-}SnMe_3]$ (**M1**), $[K(18\text{-C-6})\text{-}H_3CSnMe_2]$ (**M2**), and $[Me_3Sn{-}K(18\text{-C-6})\text{-}H_3CSnMe_2]^-$ (**M3**). The relative intensities revealed only one motif to be dominant, with a third motif to be almost negligible at 298 K.

A close inspection of Figure 7 revealed a number of cross peaks due to chemical exchanges among the trimethylstannyl species (for details see Supporting Information Figure S1). Thus, chemical exchanges were observed between the major peak at −0.47 ppm and the signals at 0.14, 0.01, −0.03, −0.08, and −0.21 ppm, and between 0.14 and 0.01 ppm, −0.08 and 0.01 ppm, and −0.08 and −0.15 ppm. All together, six signals are expected due to the methyl groups in different chemical environments in structure motifs **M1**, **M2**, and **M3**. The observed cross peaks can be explained by assuming chemical exchange among **M1**, **M2**, and **M3**. The $^1$H signal at 0.06 ppm showed that neither NOE contact nor exchange with any other peaks may due to the existence of a fourth structure motif, namely the separate ion pair $[K(18\text{-C-6})(THF)_2]^+[SnMe_3]^-$ (**M4**) in THF solution.

In tol-$d_8$ at 298 and 323 K, the $^1$H spectra of complex **2** show one sharp peak and two relative broad peaks for the 18-C-6 and $SnMe_3$ moieties, respectively. At 298 K, the signal at 3.29 ppm for 18-C-6 moieties shows NOE contacts with both peaks at 0.54 and 0.25 ppm for the $SnMe_3$ moieties, while cross peaks between the latter due to chemical exchange are observed (see Supporting Information Figure S2).[20]

It is well-known that PFG diffusion experiments provide us with the hydrodynamic radii of molecules and thus their aggregates in solution.[10,27] To verify the assumed structural motifs **M1**−**M4** and possible higher aggregates, we performed PFG diffusion measurements on **2** in THF-$d_8$ (sample **A**) at 193 and 298 K and in tol-$d_8$ (sample **B**) at 298 and 323 K.

In PFG diffusion experiments signal attenuation versus gradient strength and diffusion delay is measured, and the results are presented as Stejskal−Tanner plots.[10b] Figure 8

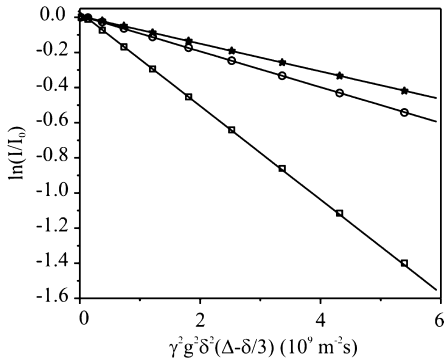


**Figure 8.** Stejskal−Tanner plots obtained from $^1$H PFG DSE diffusion experiments of complex **2** in THF-$d_8$ at 193 K of $[SnMe_3]^-$ (○), $[K(18\text{-C-6})]^+$ (★), and THF (□). The solid lines represent linear least-squares fits to the experimental data.

shows the Stejskal−Tanner plots obtained by the $^1$H PFG double-stimulated-echo (DSE) experiment on sample **A** at 193 K in THF-$d_8$. For the trimethylstannyl species the result of the signal at −0.47 ppm is presented. The slope of the signal attenuation represents the diffusion coefficient.

For a reliable analysis of molecular size on the basis of the measured diffusion coefficients, the intrinsic viscosity of the sample for diffusion experiments must be determined accurately. Thus, in both samples **A** and **B**, traces of TMS were added. Furthermore, two dummy samples containing THF-$d_8$ with trace TMS (sample **a**) and tol-$d_8$ with trace TMS (sample **b**) were prepared, and diffusion measurements at the corresponding temperatures were performed. TMS was used as internal reference for sample viscosity. Thus, by comparing the measured diffusion coefficient of TMS in samples **a** and **b** with those in samples **A** and **B**, the viscosity changes in the samples **A** and **B** (caused by adding complex **2** to the solvents) with respect to samples **a** and **b** were corrected for each sample condition, respectively. Comparison of the diffusion coefficients of the solvent signals between the respective samples was used as a cross check. In this way, the actual viscosity of samples **A** and **B** was determined at each experimental condition.

From the measured diffusion coefficients, the sizes of molecules or aggregates are usually calculated by using the


dx.doi.org/10.1021/ic500065s | Inorg. Chem. 2014, 53, 4400−4410

Table 4. Diffusion Coefficients: Observed $D_{obs}$ and Calculated $D_{cal}$ ($10^{-9}$ m$^2$ s$^{-1}$), Molecular Radii $r$ (Å), and Shape Factor $F$ of [K(18-C-6)SnMe$_3$] (2) in THF

| peak/species | $r^b$ | $F^a$ | 193 K | | 298 K | |
|---|---|---|---|---|---|---|
| | | | $D_{obs}$ | $D_{cal}{}^c$ | $D_{obs}$ | $D_{cal}{}^c$ |
| $SnMe_3$ | | | 0.11 | | 1.11 | |
| 18-C-6 | | | 0.09 | | 1.10 | |
| $[SnMe_3]^-$ | 2.90 | 1.00 | | 0.19 | | 1.70 |
| $[K(18\text{-C-}6)]^+$ | 4.28 | 1.00 | | 0.13 | | 1.15 |
| **2** (**M1**/**M2**) | 4.68 | 1.00 | | 0.12 | | 1.05 |
| $[K(18\text{-C-}6)(SnMe_3)_2]^-$ (**M3**) | 5.03 | 1.00 | | 0.11 | | 0.98 |
| $[K(18\text{-C-}6)(THF)_2]^+$ (**M4**) | 4.83 | 1.00 | | 0.11 | | |
| $[\mathbf{2}]_2$ (**M5**) | 5.90 | 1.06 | | 0.09 | | |

$^a F$ = shape factor, assuming cylindrical shape for the aggregate **M5** (see text for details). $^b r_m$ = molecular radii of the fragments in monomer calculated by molecular hard-sphere volume increments. $^c D_{cal}$ = diffusion coefficients calculated by Stokes–Einstein equation modified with a shape factor $F$ (see text for details).

Stokes–Einstein equation, either assuming a spherical shape or with appropriate structural models.[27a] Shape factors $F$ are thus introduced to modify the Stokes–Einstein equation by taking into consideration of the shape effect on the diffusion coefficient.[10c] Another way of analyzing the diffusion results for cases with known structure motifs in solution is to first calculate the radius of the core structures by molecular hard-sphere volume increments,[10d,15a] then calculate the diffusion coefficients under the experimental condition, and at last compare and approach the theoretical and experimental values of the diffusion coefficients of all possible aggregates. The latter was used to study the coordination modes and their aggregates of **2**. Table 4 shows results of the diffusion analysis on **2** in THF-$d_8$. It is worth mentioning that diffusion coefficients cannot distinguish between the structure motifs **M1** and **M2**, which are therefore corepresented by **2** in the table. A close inspection of Table 4 reveals (1) at 193 K, the observed diffusion coefficients of the $SnMe_3$ and K(18-C-6) moieties are different, which can be explained be the existence of structure motif **M4** (separate ion pair) in solution and (2) at this temperature, the calculated diffusion coefficient $D$ for a linear dimer of **2** $[\mathbf{2}]_2$ (**M5**) is smaller, whereas those for the structure motifs **M1**–**M4** are larger than the one observed for 18-C-6. The coexistence of **M1**–**M4** and **M5** (or other larger aggregates) can thus be deduced. (3) At 298 K, the observed $D$ for the $SnMe_3$ and 18-C-6 signals are similar and close to the calculated value for **2**, which means the existence of the structure motifs **M1** and **M2**, with almost negligible contribution of **M3**, **M4**, and **M5** or higher aggregates at this temperature. These are in agreement with the results revealed by NOESY spectrum.

A similar study was done on complex **2** in tol-$d_8$ (see Supporting Information, Table S1). At 298 K, the observed diffusion coefficients for the $SnMe_3$ and 18-C-6 signals are 1.10 and 1.07 ($\times 10^{-9}$ m$^2$ s$^{-1}$), while the calculated values for **2** (**M1**/**M2**), **M3**, **M4** (here, separate ion pair $[SnMe_3]^-$ $[K(18\text{-C-}6)]^+$, each has an independent diffusion coefficient), and **M5** (a linear dimer of **2**, $[\mathbf{2}]_2$) are 0.96, 0.84, (1.55, 1.05), and 0.72 ($\times 10^{-9}$ m$^2$ s$^{-1}$), respectively. At 323 K, the observed diffusion coefficients for $SnMe_3$ and 18-C-6 are 1.70 and 1.60 ($\times 10^{-9}$ m$^2$ s$^{-1}$), while the calculated values for **2** (**M1**/**M2**), **M3**, **M4** and **M5** are 1.44, 1.27, (2.34, 1.58), and 1.08 ($\times 10^{-9}$ m$^2$ s$^{-1}$), respectively. Comparison of these values reveals that at 298 K, the main species is **2**, with almost negligible contribution from the structure motifs **M3**, **M4**, and **M5** or higher aggregates, while at 323 K, a significant contribution from **M4** is detectable.

To summarize the results of $^1$H, NOESY, and PFG diffusion studies, the existence of equilibrium of multiple species of complex **2** in solution was observed. Species of five structure motifs **M1**–**M4** as well as **M5** (or other higher aggregates), which exist in the solid-state structure, were detected in THF at 193 K, while at and above RT, mononuclear species of **M1** or **M2**, that is, $[Me_3Sn\text{–}K(18\text{-C-}6)]$ and $[Me_2SnCH_3\text{–}K(18\text{-C-}6)]$, were observed to be dominant.

## CONCLUSION

The alkoxide-induced B–E bond cleavage (E = group 14 element) as an efficient access to $[ER_3]^-$ species was used to synthesize a series of $[K(L)SnMe_3]$ complexes. In the solid state, complexes **2** and **3**, with L = 18-C-6 and $(TMEDA)_2$, respectively, form structures composed of infinite head-to-tail chains of the unit $[K(L)SnMe_3]$, exhibiting K–$H_3$C and K–Sn interactions. In contrast, with L = $(12\text{-C-}4)_2$ separated $[K(12\text{-C-}4)_2]^+$ and $[SnMe_3]^-$ moieties are observed in the solid state. In the presence of 18-C-6 and THF as auxiliary ligands the remarkable species $[K(18\text{-C-}6)(THF)_2]^+[K(18\text{-C-}6)(SnMe_3)_2]^-$ $[\mathbf{2}(THF)]_2$ is formed, exhibiting K–$H_3$C and K–Sn interactions in the anion. Elucidating the nature of this unusual interaction computationally, it is shown that the K–$H_3$C coordination observed is not realized, primarily due to packing effects. Both the K–Sn and K–$H_3$C interactions are weak but significant interactions of similar strength and are comparable with typical H-bonds. In the system investigated the formation of the unsymmetrical $[(Me_2SnCH_3)K(18\text{-C-}6)SnMe_3]^-$ ion is favored not because of the strength of an individual K–Sn or K–$H_3$C interaction; rather, the formation of the unsymmetrical anion leads to the minimization of all weak interaction in the moiety. NMR NOESY combined with PFG diffusion studies give evidence for the presence of equilibria in solution, with all five structure motifs in THF-$d_8$ at 193 K as in the solid state, as well as the predominant presence of $[Me_3Sn\text{–}K(18\text{-C-}6)]$ and $[Me_2SnCH_3\text{–}K(18\text{-C-}6)]$ at and above room temperature.

## ASSOCIATED CONTENT

### Supporting Information

The SI available contains additional NMR spectroscopic and computational data. This material is available free of charge via the Internet at http://pubs.acs.org. Crystallographic data (excluding structure factors) for the structures reported in this paper were deposited with the Cambridge Crystallographic Data Centre as supplementary publication Nos. CCDC


dx.doi.org/10.1021/ic500065s | Inorg. Chem. 2014, 53, 4400–4410

975919−975922. Copies of the data can be obtained free of charge on application to CCDC, 12 Union Road, Cambridge CB2 1EZ, UK [Fax: +44(1223) 336−033; E-mail: deposit@ccdc.cam.ac.uk].

## AUTHOR INFORMATION


### Corresponding Authors

*E-mail: ch.kleeberg@tu-braunscheweig.de (C.K.).
*E-mail: joerg.grunenberg@tu-braunschweig.de (J.G.).
*E-mail: xie@mailer.uni-marburg.de (X.X.).


### Notes

The authors declare no competing financial interest.

## ACKNOWLEDGMENTS

Support for this work by a Liebig-Stipendium of the Fonds der Chemischen Industrie for C.K. is gratefully acknowledged. The authors thank Ms. Cindy Döring for help with the laboratory work. X.X. thanks the Deutsche Forschungsgemeinschaft for funding the NMR spectrometer.

## REFERENCES


(1) For an overview and selected examples, see: (a) Riviere, P.; Castel, A.; Riviere-Baudet, M. Alkaline and Alkaline Earth Metal-14 Compounds: Preparation, Spectroscopy and Reactivity. In *The Chemistry of Organo-Germanium, Tin, and Lead Compounds;* Rappoport, Z., Ed.; John Wiley & Sons: Chichester, U.K., 2002; p 653. (b) Aylett, B. J. The Main Group Elements: Group IV and V. In *Organometallic Compounds;* Coats, G. E., Aylett, B. J., Green, M. L. H., Mingos, D. M. P., Wade, K., Eds.; **1979**, Vol. *1*, part 2, p 264. (c) Weickgenannt, A.; Oestreich, M. *Chem.—Eur. J.* **2010**, *16*, 402−412.

(2) (a) Birchall, T.; Vetrone, J. A. *J. Chem. Soc., Chem. Commun.* **1988**, 877−879. (b) Buncel, E.; Gordon, R. D.; Venkatachalam, T. K. *J. Organomet. Chem.* **1996**, *507*, 81−83. (c) Reed, D.; Stalke, D.; Wright, D. S. *Angew. Chem., Int. Ed. Engl.* **1991**, *30*, 1459−1460; *Angew. Chem.* **1991**, *103*, 1539−1540. (d) Eichler, B. E.; Phillips, A. D.; Power, P. P. *Organometallics* **2003**, *22*, 5423−5426. (e) Englich, U.; Ruhlandt-Senge, K.; Uhlig, F. *J. Organomet. Chem.* **2000**, *613*, 139−147. (f) Buncel, E.; Venkatachalam, T. K.; Edlund, U.; Eliasson, B. *J. Chem. Soc., Chem. Commun.* **1984**, 1476−1477. (g) Edlund, U.; Lejon, T.; Pyykkö, P.; Venkatachalam, T. K.; Buncel, E. *J. Am. Chem. Soc.* **1987**, *109*, 5982−5985.

(3) (a) Hitchcock, P. B.; Lappert, M. F.; Lawless, G. A.; Royo, B. *J. Chem. Soc., Chem. Commun.* **1993**, 554−555. (b) Schollmeier, T.; Englich, U.; Fischer, R.; Prass, I.; Ruhlandt, K.; Schürmann, M.; Uhlig, F. *Z. Naturforsch.* **2004**, *59b*, 1462−1470.

(4) (a) Kleeberg, C. *Dalton Trans.* **2013**, *42*, 8276−8287. (b) Kleeberg, C.; Borner, C. *Eur. J. Inorg. Chem.* **2013**, 2799−2806.

(5) See for example: (a) Ma, J. C.; Dougherty, D. A. *Chem. Rev.* **1997**, *97*, 1303−1324. (b) Cabarcos, O. M.; Weinheimer, C. J.; Lisy, J. M. *J. Chem. Phys.* **1998**, *108*, 5151−5154. (c) Meyer, E. A.; Castellano, R. K.; Diederich, F. *Angew. Chem., Int. Ed.* **2003**, *42*, 1210−1250; *Angew. Chem.* **2003**, *115*, 1244−1287. (d) Dougherty, D. A. *Science* **1996**, *271*, 163−168.

(6) (a) O'Brien, J. M.; Hoveyda, A. H. *J. Am. Chem. Soc.* **2011**, *133*, 7712−7715. (b) Ito, H.; Horita, Y.; Yamamoto, E. *Chem. Commun.* **2012**, 8006−8008. (c) Yamamoto, E.; Izumi, K.; Horita, Y.; Ito, H. *J. Am. Chem. Soc.* **2012**, *134*, 19997−20000. (d) Mita, T.; Chen, J.; Sugawara, M.; Sato, Y. *Org. Lett.* **2012**, *14*, 6202−6205. (e) Kawachi, A.; Minamimoto, T.; Tamao, K. *Chem. Lett.* **2001**, 1216−1217.

(7) Kleeberg, C. *Z. Anorg. Allg. Chem.* **2011**, *637*, 1790−1794.

(8) Fulmer, G. R.; Miller, A. J. M.; Sherden, N. H.; Gottlieb, H. E.; Nudelman, A.; Stoltz, B. M.; Bercaw, J. E.; Goldberg, K. I. *Organometallics* **2010**, *29*, 2176−2179.

(9) (a) Wagner, R.; Berger, S. *J. Magn. Reson., Ser. A* **1996**, *123*, 119−121. (b) Baumann, R.; Wider, G.; Ernst, R. R.; Wütherich, K. *J. Magn. Reson.* **1981**, *44*, 402−406. (c) Bax, A.; Davis, D. G. *J. Magn. Reson.* **1985**, *63*, 207−213. (d) Jeener, J.; Meier, B. H.; Bachmann, P.; Ernst, R. R. *J. Chem. Phys.* **1979**, *71*, 4546−4553.

(10) (a) Jerschow, A.; Müller, N. *J. Magn. Reson., Ser. A* **1997**, *125*, 372−375. (b) Tanner, J. E. *J. Chem. Phys.* **1970**, *52*, 2523−2526. (c) Bloomfield, V. A. Separation and Hydrodynamics. In *Biophysics Textbook Online;* Schuster, T. M., Ed.; Biophysical Society: Bethesda, MD, **2000**; pp 1−5. (d) Ben-Amotz, D.; Willis, K. G. *J. Phys. Chem.* **1993**, *97*, 7736−7742.

(11) (a) Stalke, D. *Chem. Soc. Rev.* **1998**, *27*, 171−178. (b) *CrysAlisPro,* Version 1.171.34.44−1.171.36.24; Agilent Technologies: Santa Clara, CA, 2010−2012. (c) Sheldrick, G. M. *Acta Crystallogr.* **2008**, *A64*, 112−122. (d) Farrugia, L. J. *J. Appl. Crystallogr.* **1999**, *32*, 837−838. (e) Spek, A. L. *PLATON*—A Multipurpose Crystallographic Tool; Utrecht University: Utrecht, The Netherlands, 1998. (f) Macrae, C. F.; Bruno, I. J.; Chisholm, J. A.; Edgington, P. R.; McCabe, P.; Pidcock, E.; Rodriguez-Monge, L.; Taylor, R.; van de Streek, J.; Wood, P. A. *J. Appl. Crystallogr.* **2008**, *41*, 466−470. (g) Brandenburg, K. *Diamond 3.2i;* Crystal Impact GbR: Bonn, Germany, 1997.

(12) Weber, L.; Domke, I.; Greschner, W.; Miqueu, K.; Chrostowska, A.; Baylère, P. *Organometallics* **2005**, *24*, 5455−5463.

(13) Despite considerable efforts we are unable to provide a satisfactory elemental analysis for **3** as this compound decomposes readily upon drying *in vacuo*, possibly induced by loss of TMEDA. See Experimental Section for details.

(14) All individual crystals considered were nonmerohedrally twinned. For the selected crystal a solution was established on the basis of the data of one domain, and the refinement was carried out with data of both domains. For further details see the deposited data (CCDC 975922).

(15) (a) Bondi, A. *J. Phys. Chem.* **1964**, *68*, 441−452. (b) *CRC Handbook of Chemistry and Physics*, 57$^{th}$ ed.; Weast, R. C., Ed.; CRC Press, Inc.: Cleveland, OH, 1976−1977.

(16) Alternatively a van der Waals radius of 2.0 Å for a methyl group may be considered, resulting in a sum of van der Waals radii of 4.75 Å (K−CH3) and, hence, an even more peculiar difference of 1.57 Å to the observed distance K1−C3.

(17) A search in the CSD database (Version 5.34, Nov 2012) revealed that 938 [98] structures have been deposited with K−C distances below 4.45 Å within K−$H_3C$ substructures [containing a $[K(18\text{-}C\text{-}6)]^+$ fragment]. Of these structures 230 [33] have K−$H_3C$ distances comparable to the compounds discussed here of below 3.5 Å.

(18) (a) Teng, W.; Ruhlandt-Senge, K. *Chem.—Eur. J.* **2005**, *11*, 2462−2470. (b) Jenkins, D. M.; Teng, W.; Englich, U.; Stone, D.; Ruhlandt-Senge, K. *Organometallics* **2001**, *20*, 4600−4606.

(19) (a) Wolstenholme, D. J.; Prince, P. D.; McGrady, G. S.; Landry, M. J.; Steed, J. W. *Inorg. Chem.* **2011**, *50*, 11222−11227. (b) Pritzkow, H.; Lobreyer, T.; Sundermeyer, W.; van Eikema Hommes, N. J. R.; von Ragué Schleyer, P. *Angew. Chem., Int. Ed.* **1994**, *33*, 216−217; *Angew. Chem.* **1994**, *106*, 221−223.

(20) See Supporting Information for details.

(21) Furthermore, three of four crystallographically independent TMEDA moieties within the asymmetric unit show positional disorder over two sites. Both disordered moieties ($SnMe_3$ and TMEDA) were refined by employing split atom models refining a common anisotropic displacement parameter for each disordered atom pair (no restraints employed). The site occupancy factor refined for each individual disordered moiety refined to 0.7; hence, a common SOF appeared chemically and crystallographically sensible and refined to 0.6959(9). For further details see the crystallographic data (CCDC 975921).

(22) (a) Zhao, Y.; Truhlar, D. G. *Acc. Chem. Res.* **2008**, *41*, 157−167. (b) Weigend, F.; Ahlrichs, R. *Phys. Chem. Chem. Phys.* **2005**, *7*, 3297−3305. (c) Leininger, T.; Nicklass, A.; Kuechle, W.; Stoll, H.; Dolg, M.; Bergner, A. *Chem. Phys. Lett.* **1996**, *255*, 274−280. (d) Frisch, M. J.; Trucks, G. W.; Schlegel, H. B.; Scuseria, G. E.; Robb, M. A.; Cheeseman, J. R.; Scalmani, G.; Barone, V.; Mennucci, B.; Petersson, G. A.; Nakatsuji, H.; Caricato, M.; Li, X.; Hratchian, H. P.; Izmaylov, A. F.; Bloino, J.; Zheng, G.; Sonnenberg, J. L.; Hada, M.; Ehara, M.; Toyota, K.; Fukuda, R.; Hasegawa, J.; Ishida, M.; Nakajima, T.; Honda,

Y.; Kitao, O.; Nakai, H.; Vreven, T.; Montgomery, Jr., J. A.; Peralta, J. E.; Ogliaro, F.; Bearpark, M.; Heyd, J. J.; Brothers, E.; Kudin, K. N.; Staroverov, V. N.; Kobayashi, R.; Normand, J.; Raghavachari, K.; Rendell, A.; Burant, J. C.; Iyengar, S. S.; Tomasi, J.; Cossi, M.; Rega, N.; Millam, J. M.; Klene, M.; Knox, J. E.; Cross, J. B.; Bakken, V.; Adamo, C.; Jaramillo, J.; Gomperts, R.; Stratmann, R. E.; Yazyev, O.; Austin, A. J.; Cammi, R.; Pomelli, C.; Ochterski, J. W.; Martin, R. L.; Morokuma, K.; Zakrzewski, V. G.; Voth, G. A.; Salvador, P.; Dannenberg, J. J.; Dapprich, S.; Daniels, A. D.; Farkas, Ö.; Foresman, J. B.; Ortiz, J. V.; Cioslowski, J.; Fox, D. J. *Gaussian 09, Revision A.1;* Gaussian, Inc.: Wallingford, CT, 2009. (e) Brandhorst, K.; Grunenberg, J. *J. Chem. Phys.* **2010**, *132*, 184101−184107.

(23) Brandhorst, K.; Grunenberg, J. *Chem. Soc. Rev.* **2008**, *37*, 1558−1567.

(24) For a detailed discussion and recent examples for the utility of compliance constants, see: (a) Grunenberg, J.; Barone, G. *RSC Adv.* **2013**, *3*, 4757−4762. (b) von Frantzius, G.; Espinosa Ferao, A.; Streubel, R. *Chem. Sci.* **2013**, *4*, 4309−4322. (c) Markopoulos, G.; Grunenberg, J. *Angew. Chem., Int. Ed.* **2013**, *52*, 10648−10651; *Angew. Chem.* **2013**, *125*, 10842−10845.

(25) Grunenberg, J. *J. Am. Chem. Soc.* **2004**, *126*, 16310−16311.

(26) (a) Schneider, H.-J. *Angew. Chem., Int. Ed.* **2009**, *48*, 3924−3977; *Angew. Chem.* **2009**, *121*, 3982−4036. (b) Grunenberg, J. *Phys. Chem. Chem. Phys.* **2011**, *13*, 10136−10146.

(27) For selected examples, see: (a) Xie, X.; Auel, C.; Henze, W.; Gschwind, R. M. *J. Am. Chem. Soc.* **2003**, *125*, 1595−1601. (b) Schlörer, N. E.; Cabrita, E. J.; Berger, S. *Angew. Chem., Int. Ed.* **2002**, *41*, 107−109; *Angew. Chem.* **2002**, *114*, 114−116. (c) Keresztes, I.; Williard, P. G. *J. Am. Chem. Soc.* **2000**, *122*, 10288−10229. (d) Beck, S.; Geyer, A.; Brintzinger, H.-H. *Chem. Commun.* **1999**, 2477−2478. (e) Armstrong, D. R.; García-Álvarez, P.; Kennedy, A. R.; Mulvey, R. E.; Robertson, S. D. *Chem.—Eur. J.* **2011**, *17*, 6725−6730. (f) García-Álvarez, P.; Mulvey, R. E.; Parkinson, J. A. *Angew. Chem., Int. Ed.* **2011**, *50*, 9668−9671; *Angew. Chem.* **2011**, *123*, 9842−9845. (g) Cohen, Y.; Avram, L.; Frish, L. *Angew. Chem., Int. Ed.* **2005**, *44*, 520−554; *Angew. Chem.* **2005**, *117*, 524−560.